tvst

Retina

Artificial Intelligence–Assisted Perfusion Density as Biomarker for Screening Diabetic Nephropathy

Xiao Xie[1–3,*], Wenqi Wang[4,*], Hongyan Wang[1–3], Zhiping Zhang[5], Xiaomeng Yuan[1–3], Yanmei Shi[5], Yanfeng Liu[6], Qingjun Zhou[2,7], and Tingting Liu[1–3]

[1] Eye Institute of Shandong First Medical University, Eye Hospital of Shandong First Medical University (Shandong Eye Hospital), Jinan, China
[2] State Key Laboratory Cultivation Base, Shandong Provincial Key Laboratory of Ophthalmology, Qingdao, China
[3] School of Ophthalmology, Shandong First Medical University, Jinan, China
[4] Department of Chinese Medicine Ophthalmology, The First Affiliated Hospital of Shandong First Medical University (Shandong Provincial Qianfoshan Hospital), Jinan, China
[5] First Clinical Medical College, Shandong University of Traditional Chinese Medicine, Jinan, China
[6] Jinan Health Care Center for Women and Children, Jinan, China
[7] Qingdao Eye Hospital of Shandong First Medical University, Qingdao, China

Correspondence: Tingting Liu, Eye Hospital of Shandong First Medical University (Shandong Eye Hospital), Jinan 250021, China. e-mail: tingtingliu@vip.sina.com

Received: December 6, 2023
Accepted: July 30, 2024
Published: October 10, 2024

Keywords: diabetic retinopathy; diabetic nephropathy; ultra-widefield; swept-source optical coherence tomography angiography; perfusion density; artificial intelligence

Citation: Xie X, Wang W, Wang H, Zhang Z, Yuan X, Shi Y, Liu Y, Zhou Q, Liu T. Artificial intelligence–assisted perfusion density as biomarker for screening diabetic nephropathy. Transl Vis Sci Technol. 2024;13(10):19, https://doi.org/10.1167/tvst.13.10.19

Purpose: To identify a reliable biomarker for screening diabetic nephropathy (DN) using artificial intelligence (AI)–assisted ultra-widefield swept-source optical coherence tomography angiography (UWF SS-OCTA).

Methods: This study analyzed data from 169 patients (287 eyes) with type 2 diabetes mellitus (T2DM), resulting in 15,211 individual data points. These data points included basic demographic information, clinical data, and retinal and choroidal data obtained through UWF SS-OCTA for each eye. Statistical analysis, 10-fold cross-validation, and the random forest approach were employed for data processing.

Results: The degree of retinal microvascular damage in the diabetic retinopathy (DR) with the DN group was significantly greater than in the DR without DN group, as measured by SS-OCTA parameters. There were strong associations between perfusion density (PD) and DN diagnosis in both the T2DM population ($r = -0.562$ to -0.481, $P < 0.001$) and the DR population ($r = -0.397$ to -0.357, $P < 0.001$). The random forest model showed an average classification accuracy of 85.8442% for identifying DN patients based on perfusion density in the T2DM population and 82.5739% in the DR population.

Conclusions: Quantitative analysis of microvasculature reveals a correlation between DR and DN. UWF PD may serve as a significant and noninvasive biomarker for evaluating DN in patients through deep learning. AI-assisted SS-OCTA could be a rapid and reliable tool for screening DN.

Translational Relevance: We aim to study the pathological processes of DR and DN and determine the correspondence between their clinical and pathological manifestations to further clarify the potential of screening DN using AI-assisted UWF PD.

Introduction

Diabetic retinopathy (DR) and diabetic nephropathy (DN) are common microvascular complications of type 2 diabetes mellitus (T2DM) and can affect the macula and peripheral retina, leading to blindness in critically ill or end-stage renal disease patients.[1–3] Therefore, the early diagnosis of DR and DN is very important to prevent blindness in these patients.

In recent years, rapid advancements in imaging technology have enabled dynamic, multilevel, three-dimensional, and high-resolution observation of the

retina and choroid. Given the close relationship between the pathophysiological mechanisms and clinical changes of DN and DR,[2,4] researchers believe that these conditions can predict each other.[2,5,6] Previous studies have explored the correlation between DN and fundus images or blood flow in the macular region, finding that renal impairment is linked to the enlargement of the foveal avascular zone (FAZ) in diabetic patients.[7,8] However, microvascular lesions in DR are not confined to the macular fovea but are widespread throughout the retinal microvasculature. In this context, swept-source optical coherence tomography angiography (SS-OCTA) allows for the quick, highly detailed, and noninvasive quantification of a wide range of retinal features.[9] Our preliminary SS-OCTA studies confirm that this technology provides valuable information for detecting potential blood flow damage at various stages of DR.[10]

Currently, the clinical diagnostic criteria for DN rely primarily on invasive serological examinations and renal biopsies.[11] Retinal screening for DN in T2DM patients is typically limited to fundus imaging and the FAZ evaluation, which do not provide comprehensive quantification of retinal and choroidal microvasculature characteristics. Additionally, due to the abnormal renal function in DN patients, invasive fluorescein fundus angiography (FFA) cannot be used to assess retinal and choroidal microvasculature damage. We hypothesized that certain parameters from the ultra-widefield (UWF) SS-OCTA could serve as rapid, noninvasive, and reliable screening biomarkers for DN.

To test this hypothesis, we conducted a prospective study to observe retinal and choroidal microvasculature characteristics in patients with DR and DN using UWF SS-OCTA. We then classified the data using a random forest model to distinguish DN patients from the T2DM population (including a control group, a DR without DN group, and a DR with DN group) and the DR population (including a DR without DN group and a DR with DN group). The goal is to provide real-time monitoring for DR patients and assess the presence of DN using artificial intelligence (AI)–assisted UWF parameters. This approach aims to identify a quick, noninvasive, and reliable biomarker for DN screening.

Methods

General Information

This study included a total of 169 patients with T2DM who were treated at the Shandong Eye Hospital from November 2020 to May 2022. The study protocol was approved by the Institutional Review Board of Shandong Eye Hospital (approval No. SDSYKYY202105). Written informed consent was obtained from all participating patients. All patients' demographics and basic clinical characteristics were recorded. Patients without any systemic diseases or retinopathy were included in the healthy group. Patients with T2DM[12] and meeting the diagnostic criteria of DR[13] were allotted to the DR without DN group. Patients with T2DM[12] and meeting the diagnostic criteria of DR[13] but not of DN[14,15] were included in the DR with DN group.

Machines for Eye Examination

All the patients were examined by an experienced physician using UWF SS-OCTA (SS-OCT, VG200D; SVision Imaging, Ltd, Luo Yang, China). The commercial SS-OCT equipment contained an SS laser with a central wavelength of approximately 1050 nm (full width of 990–1100 nm) and a scanning rate of 200,000 A-scans per second. The full width of the half-maximum axial resolution of the device in tissue was approximately 5 µm, and the estimated lateral resolution on the retinal surface was approximately 15 µm.[16] Both optical coherence tomography (OCT) and OCTA data of 21 × 21 mm^2 area centered on the macular fovea were obtained by 1024 (horizontal) × 1024 (vertical) B-scans. By using the built-in eye-tracking mode of the device based on the integrated confocal scanning laser detector lens, eye movement artifacts during and between scans were minimized.[17]

Data Extraction and Deep Learning Analysis

The built-in AI identification and quantification software of the SS-OCTA recorded the area, perimeter and acircularity index, and fractal dimension 300 (FD300; blood flow density within a radius of 300 µm around FAZ)[18] of FAZ, total retinal thickness (RT) (measured from the internal limiting membrane to the retinal pigment epithelium [RPE] in the central subfield),[19] retinal vessel density (VD) and perfusion density (PD) of the deep vascular complex, choroidal perfusion (CP), choroidal vascularity volume (CVV; defined as the volume of the large and medium choroidal vessels), choroidal vascularity index (CVI; defined as the ratio of the volume of the large and medium choroidal vessels to the total choroidal volume), and choroidal thickness (CT) (measured from the outer edge of the hyperreflective RPE line to the inner edge of the sclera) in different circular radii

around the fovea.[19–22] Data collection was carried out independently by an experienced investigator.

Automatic measurement using SS-OCT built-in software offers an effective and objective method for quantitatively evaluating retinal and choroidal structures. Typically, the system's default hierarchical mode was used, with manual corrections made for any segmentation errors. However, scan artifacts present substantial challenges to accurate quantification of the retinal and choroidal layers.[23,24] To address this, the image quality score (IQS) of SS-OCTA images was assessed, and images with scores below 8 were excluded to eliminate large errors caused by projection, bulk motion, signal reduction, and other issues.[23] This evaluation was performed by two experienced ophthalmologists who were kept blinded to the participants' data. In cases of disagreement, a more experienced ophthalmologist made the final decision. Samples with IQS scores below 8, which could not be corrected manually due to segmentation errors, motion artifacts, defocus, decentration, and masking, were excluded.

A deep learning method was employed to standardize the data, selecting the most relevant optimal OCT parameters through 10-fold cross-validation (expressed by the importance of explanatory variables). Then, the data were randomly divided into 10 groups with approximately equal numbers to form a training set and a test set. The training set was divided into 10 folds for cross-validation, with each fold containing 90% training data and 10% verification data.[25] Finally, the training set data were then fitted to a random forest model, which was used to classify the data from the testing set.[26] Based on the optimal OCT parameters, we identified DN patients (DR with DN group) from the T2DM population (control group, DR without DN group, DR with DN group) and the DR population (DR without DN group, DR with DN group) and calculated the classification accuracy. All results were evaluated through a 10-fold cross-validation.[27]

The obtained data were also statistically analyzed using SPSS v26.0 (SPSS, Inc., Chicago, IL, USA). The data were tested for normal distribution, followed by one-way analysis of variance or Kruskal–Wallis test (H test) as appropriate. Bonferroni correction was applied for multiple comparisons. Additionally, the Spearman correlation coefficient was used to evaluate the relationship between OCT parameters and grouping categories.

Results

Patient Characteristics

The baseline demographic and clinical characteristics of the enrolled patients are summarized in Table 1. In this study, data from 169 patients (287 eyes) with T2DM were analyzed, comprising 15,211 individual data points. Ninety-eight control subjects (162 eyes) without retinal microvascular lesions were recruited, comprising 45 males and 53 females. Retinal microvascular lesions were identified in 71 subjects (125 eyes). There was a significant difference in gender distribution among the three groups ($\chi^2 = 6.978$, $P = 0.031$). The average ages of patients among the control, DR without DN, and DR with DN groups were 54.31 ± 11.27 (range, 23–72), 56.76 ± 9.91 (range, 32–75), and 56.00 ± 9.67 (range, 39–79) years, respectively. There was no significant difference ($F = 0.524$, Bonferroni corrected $P = 0.694$). Patients in the control group did not have T2DM. The duration of T2DM in the DR without DN group (mean ± SD = 9.53 ± 6.71) was significantly shorter than that in the DR with DN group (mean ± SD = 13.31 ± 6.40) ($t = -2.399$, $P = 0.02$).

Our results indicated that the best-corrected visual acuity (BCVA) measured using the international standard chart of vision and recorded as the logarithmic minimum angle of resolution (logMAR) was worse

Table 1. Demographic and Clinical Characteristics of Enrolled Patients

Variable	Control Group	DR Without DN Group	DR With DN Group	$\chi^2/F/t$ Test	Bonferroni Correction
N (subjects/eyes)	98/162	42/75	29/50		
Gender (male/female)	45/53	27/15	20/9	$\chi^2 = 6.978$	$P = 0.031^*$
Age, y	54.31 ± 11.27	56.76 ± 9.91	56.00 ± 9.67	$F = 0.524$	$P = 0.694$
Duration of diabetes, y	0 ± 0	9.53 ± 6.71	13.31 ± 6.40	$t = -2.399$	$P = 0.02^*$
BCVA (logMAR)	0.02 ± 0.04	0.30 ± 0.29	0.59 ± 0.42	$H = 91.827$	$P < 0.001^{**}$
IOP	15.24 ± 1.95	15.39 ± 2.55	15.56 ± 2.56	$H = 0.759$	$P = 0.684$

IOP, intraocular pressure.
$^*P \leq 0.05$, $^{**}P \leq 0.001$.

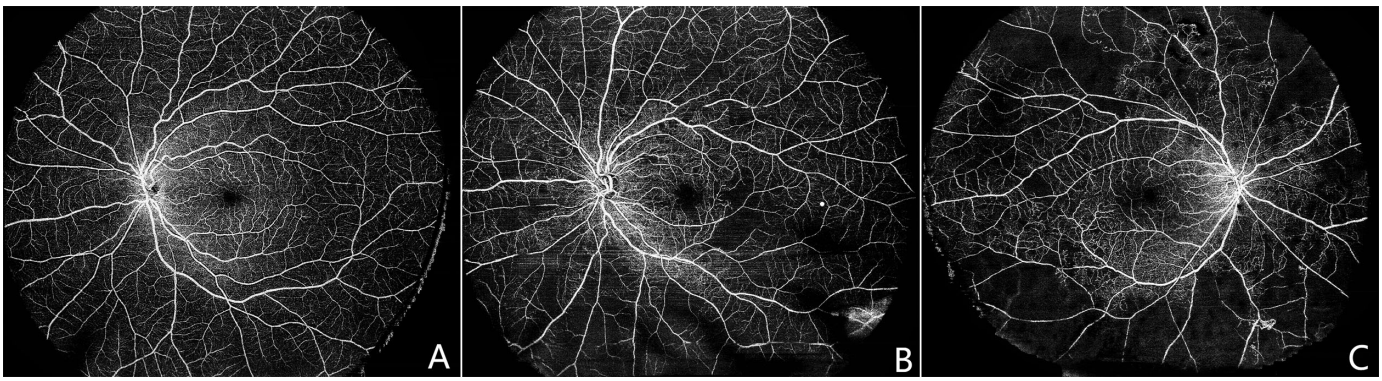

Figure 1. The ultra-widefield fundus vascular images of retinal vascular complexes. The fundus vascular images of deep vascular complex in the control (**A**), DR without DN (**B**), and DR with DN (**C**) groups.

Table 2. The Characteristics of FAZ in the Control, DR Without DN, and DR With DN Groups Using UWF SS-OCTA.

Variable	Control Group	DR Without DN Group	DR With DN Group	*F* or *H* Test	Bonferroni Correction
FAZ area, mm^2	0.38 ± 0.08	0.43 ± 0.15	0.51 ± 0.18	$H = 13.397$	$P = 0.001^{***}$
FAZ perimeter, mm	2.58 ± 0.32	2.79 ± 0.56	3.09 ± 0.74	$H = 11.344$	$P = 0.003^{**}$
FAZ acircularity index	0.71 ± 0.09	0.93 ± 0.28	0.99 ± 0.30	$H = 16.236$	$P < 0.001^{***}$
FAZ FD300, mm^{-1}	42.71 ± 5.37	42.2 ± 6.98	38.72 ± 7.35	$H = 5.757$	$P = 0.056$

$^{**}P \leq 0.01$, $^{***}P \leq 0.001$.

in the DR without DN group (mean ± SD = 0.30 ± 0.29) and DR with DN group (mean ± SD = 0.59 ± 0.42) compared to the control group (mean ± SD = 0.02 ± 0.04). The BCVA was significantly poorer in the DR with DN group ($H = 91.827$, Bonferroni corrected $P < 0.001$). There was no significant difference in intraocular pressure among the three groups (mean ± SD = 15.24 ± 1.95, 15.39 ± 2.55, and 15.56 ± 2.56; $H = 0.759$, $P = 0.684$).

Retinal Vascular Complexes

In the UWF vascular images of the deep retinal vascular complexes (Fig. 1), the control group exhibited evenly distributed and densely packed blood vessels. In contrast, patients with DR showed nonperfusion areas, with significantly larger areas observed in those with DN.

As depicted in Table 2 and Figure 2A, compared to the control group, the area ($H = 13.397$, Bonferroni corrected $P = 0.001$), perimeter ($H = 11.344$, Bonferroni corrected $P = 0.003$), and acircularity index ($H = 16.236$, Bonferroni corrected $P < 0.001$) of the FAZ were significantly increased in both the DR without DN and DR with DN groups. However, there was no significant difference in the FD300 of FAZ among the three groups ($H = 5.757$; Bonferroni corrected $P = 0.056$).

In Table 3 and Figures 2B–D, we compared the PD and VD of the deep vascular complex and RT across various circular radii centered on the macular fovea. Except for $PD_{0-1\ mm}$ and $VD_{0-1\ mm}$, significant differences in PD and VD of the deep vascular complex were found across different radii among the three groups (Bonferroni corrected $P < 0.001$). Both the average PD and VD were significantly decreased in the DR without DN and DR with DN groups compared to the control group. Moreover, the reduction in PD and VD in the DR with DN group was notably more pronounced than in the DR without DN group within certain radii. Moreover, significant differences in $RT_{0-3\ mm}$ ($H = 11.272$, Bonferroni corrected $P = 0.004$), $RT_{0-6\ mm}$ ($H = 28.986$, Bonferroni corrected $P < 0.001$), $RT_{0-9\ mm}$ ($H = 22.306$, Bonferroni corrected $P < 0.001$), and $RT_{0-12\ mm}$ ($H = 10.861$, Bonferroni corrected $P = 0.004$) were observed among the three groups. The mean RT values in both DR without DN and DR with DN groups were significantly higher compared to the control group.

Our figure and data analysis revealed varying degrees of damage in the retinal vascular complex among patients in the DR without DN and DR with

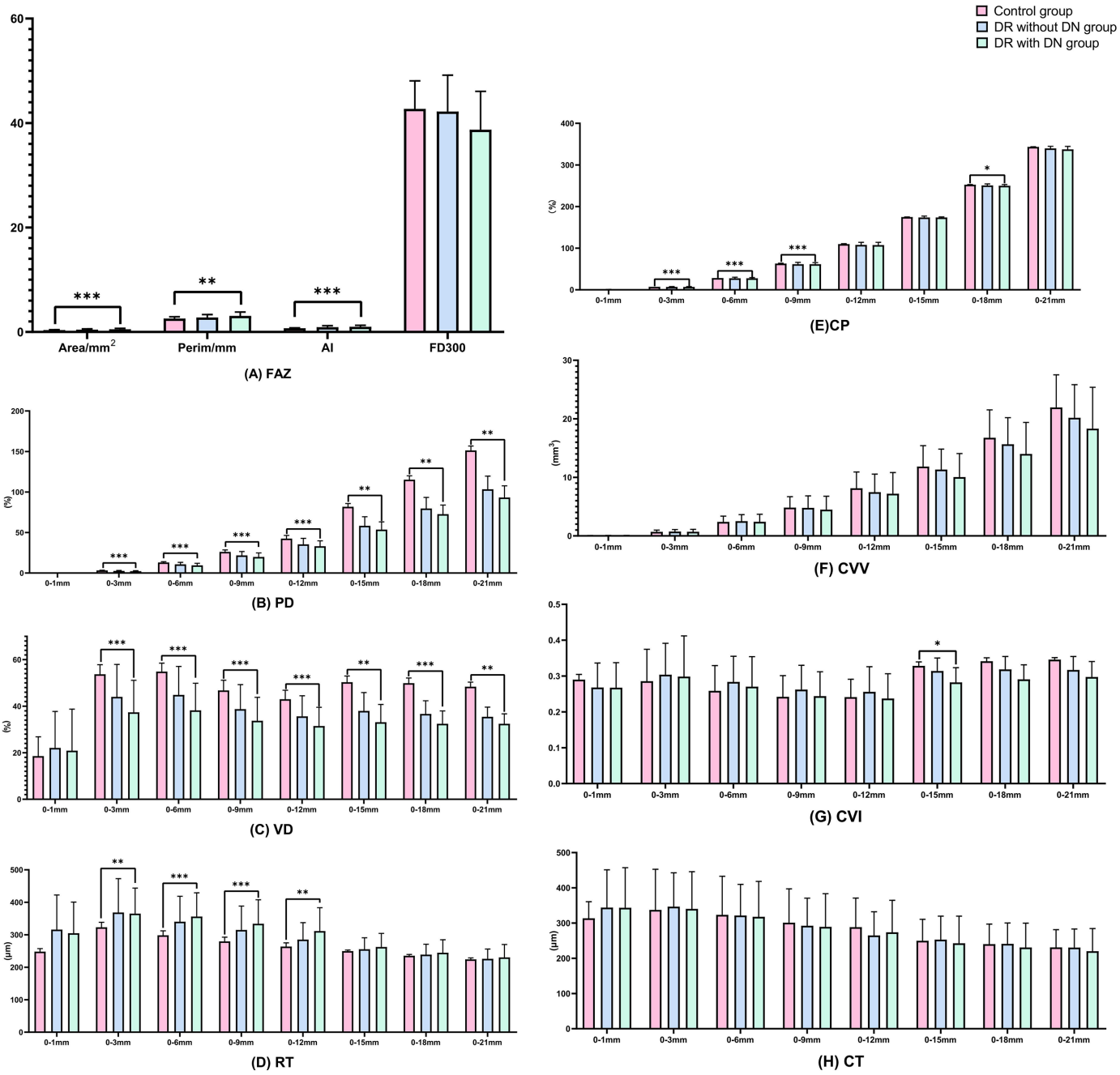

Figure 2. The OCTA parameters in the control, DR without DN, and DR with DN using UWF SS-OCTA. Comparison of the area, perimeter, acircularity index, and fractal dimension of FAZ (**A**), PD (**B**), VD (**C**), RT (**D**), CP (**E**), CVV (**F**), CVI (**G**), and CT (**H**) in different radii at the center of the macular fovea. $^{*}P \leq 0.05$, $^{**}P \leq 0.01$, $^{***}P \leq 0.001$.

DN groups, particularly in PD and VD, with the DR with DN group exhibiting more severe damage.

Choroidal Vascular Complexes

In Table 4 and Figures 2E–H, we compared the mean values of choroidal parameters (CP, CVV, CVI, and CT) across different circular radii centered on the macular fovea for all included subjects.

Significant differences were observed among the three groups in $CP_{0-3\ mm}$ ($H = 23.255$, Bonferroni corrected $P < 0.001$), $CP_{0-6\ mm}$ ($H = 23.645$, Bonferroni corrected $P < 0.001$), $CP_{0-9\ mm}$ ($H = 20.901$, $P < 0.001$), $CP_{0-18\ mm}$ ($H = 7.221$, Bonferroni corrected $P = 0.027$), $CVI_{0-15\ mm}$ ($F = 5.418$, Bonferroni corrected

Table 3. The OCTA Parameters of the Retina in the Control, DR Without DN, and DR With DN Groups Using UWF SS-OCTA

Variable	Control Group	DR Without DN Group	DR With DN Group	*F* or *H* Test	Bonferroni Correction
$PD_{0-1\ mm}$	0.11 ± 0.04	0.10 ± 0.07	0.12 ± 0.08	$F = 0.176$	$P = 0.893$
$PD_{0-3\ mm}$	3.13 ± 0.26	2.50 ± 0.73	2.17 ± 0.78	$H = 50.842$	$P < 0.001^{***}$
$PD_{0-6\ mm}$	12.95 ± 1.07	10.68 ± 2.55	9.38 ± 2.64	$F = 34.797$	$P < 0.001^{***}$
$PD_{0-9\ mm}$	26.00 ± 2.53	21.64 ± 4.91	19.71 ± 5.17	$F = 28.41$	$P < 0.001^{***}$
$PD_{0-12\ mm}$	42.38 ± 4.05	35.30 ± 7.58	33.03 ± 6.69	$F = 29.626$	$P < 0.001^{***}$
$PD_{0-15\ mm}$	81.73 ± 4.04	58.17 ± 11.34	53.56 ± 9.55	$H = 11.462$	$P = 0.003^{**}$
$PD_{0-18\ mm}$	115.18 ± 4.85	79.56 ± 13.78	72.61 ± 11.34	$F = 19.745$	$P = 0.002^{**}$
$PD_{0-21\ mm}$	151.25 ± 5.55	103.32 ± 16.29	93.13 ± 14.50	$F = 24.24$	$P = 0.002^{**}$
$VD_{0-1\ mm}$	18.55 ± 8.28	22.06 ± 15.68	20.87 ± 17.87	$H = 0.096$	$P = 0.859$
$VD_{0-3\ mm}$	53.70 ± 4.11	43.99 ± 13.96	37.36 ± 13.74	$H = 47.770$	$P < 0.001^{***}$
$VD_{0-6\ mm}$	54.86 ± 3.65	44.86 ± 12.24	38.22 ± 11.64	$H = 61.115$	$P < 0.001^{***}$
$VD_{0-9\ mm}$	46.78 ± 4.38	38.75 ± 10.52	33.74 ± 10.08	$F = 28.281$	$P < 0.001^{***}$
$VD_{0-12\ mm}$	42.99 ± 3.86	35.65 ± 8.84	31.50 ± 8.03	$F = 31.092$	$P < 0.001^{***}$
$VD_{0-15\ mm}$	50.29 ± 2.70	37.96 ± 7.89	33.12 ± 7.64	$F = 9.131$	$P = 0.002^{**}$
$VD_{0-18\ mm}$	49.88 ± 2.23	36.68 ± 5.66	32.46 ± 5.49	$F = 17.602$	$P < 0.001^{***}$
$VD_{0-21\ mm}$	48.37 ± 1.99	35.45 ± 4.13	32.43 ± 4.27	$F = 25.173$	$P = 0.001^{**}$
$RT_{0-1\ mm}$	248.05 ± 9.42	315.78 ± 106.90	304.78 ± 95.81	$H = 3.325$	$P = 0.19$
$RT_{0-3\ mm}$	322.98 ± 15.44	368.61 ± 104.31	365.18 ± 78.59	$H = 11.272$	$P = 0.004^{**}$
$RT_{0-6\ mm}$	298.52 ± 13.62	340.38 ± 78.26	356.24 ± 72.87	$H = 28.986$	$P < 0.001^{***}$
$RT_{0-9\ mm}$	279.60 ± 12.90	314.91 ± 73.49	333.79 ± 74.06	$H = 22.306$	$P < 0.001^{***}$
$RT_{0-12\ mm}$	263.76 ± 11.43	285.22 ± 52.01	311.34 ± 72.02	$H = 10.861$	$P = 0.004^{**}$
$RT_{0-15\ mm}$	249.72 ± 3.23	255.67 ± 35.16	262.40 ± 41.97	$H = 0.626$	$P = 0.731$
$RT_{0-18\ mm}$	235.45 ± 3.89	238.88 ± 32.10	244.64 ± 40.00	$H = 0.469$	$P = 0.791$
$RT_{0-21\ mm}$	224.42 ± 4.53	225.84 ± 30.16	230.50 ± 39.61	$H = 0.247$	$P = 0.884$

$^{**}P \leq 0.01$, $^{***}P \leq 0.001$.

$P = 0.013$), and $CVI_{0-18\ mm}$ ($F = 5.039$, Bonferroni corrected $P = 0.01$). In comparison to the control group, the CP near the macular fovea was significantly reduced in both the DR without DN and DR with DN groups.

Correlation Between OCT Parameters and DN Diagnosis

Based on the statistical analysis and fundus image observations described above, we hypothesized that PD and VD of the deep vascular complex may serve as effective OCT parameters for screening DN. To test this hypothesis, Pearson's correlation coefficients were computed. Specifically, since the radii of 0 to 3 mm, 0 to 6 mm, 0 to 9 mm, and 0 to 12 mm are commonly used in UWF imaging, we conducted Pearson correlation analysis for OCT parameters within these ranges.

As shown in Table 5, UWF PD demonstrated stronger correlations compared to other OCT parameters when screening for DN in both the T2DM and DR populations.

Screening Results of DN by Random Forest Model

We also employed the deep learning method to standardize our data, assessing the importance of explanatory variables through 10-fold cross-validation to identify the most relevant optimal OCT parameters. The importance of these variables, as determined by the random forest model for screening DN from both the T2DM and DR populations, is detailed in Table 5 (Importance). In the classification of DN from the T2DM population, key explanatory variables included PD ($PD_{0-3\ mm}$: 0.093891, $PD_{0-6\ mm}$: 0.086285, $PD_{0-12\ mm}$: 0.251083) and VD ($VD_{0-6\ mm}$: 0.081844, $VD_{0-12\ mm}$: 0.089028). Similarly, in the classification of DN from the DR population, crucial variables were PD ($PD_{0-3\ mm}$: 0.075730, $PD_{0-6\ mm}$: 0.115155, $PD_{0-9\ mm}$: 0.079301) and VD ($VD_{0-6\ mm}$: 0.147807,

Table 4. The OCTA Parameters of Choroid in the Control, DR Without DN, and DR With DN Groups Using UWF SS-OCTA

Variable	Control Group	DR Without DN Group	DR With DN Group	*F* or *H* Test	Bonferroni Correction
$CP_{0-1\ mm}$	0.79 ± 0.00	0.75 ± 0.16	0.79 ± 0.00	$H = 0.977$	$P = 0.614$
$CP_{0-3\ mm}$	7.07 ± 0.00	6.89 ± 0.86	6.83 ± 0.94	$H = 23.255$	$P < 0.001^{***}$
$CP_{0-6\ mm}$	28.27 ± 0.05	27.69 ± 2.43	27.64 ± 1.68	$H = 23.645$	$P < 0.001^{***}$
$CP_{0-9\ mm}$	63.09 ± 0.69	61.62 ± 4.40	61.57 ± 3.69	$H = 20.901$	$P < 0.001^{***}$
$CP_{0-12\ mm}$	109.87 ± 1.08	107.96 ± 6.12	107.47 ± 6.56	$H = 2.26$	$P = 0.323$
$CP_{0-15\ mm}$	174.74 ± 0.36	173.77 ± 3.29	173.77 ± 1.38	$H = 4.873$	$P = 0.087$
$CP_{0-18\ mm}$	252.43 ± 0.43	250.76 ± 3.69	249.92 ± 3.01	$H = 7.221$	$P = 0.027^{*}$
$CP_{0-21\ mm}$	343.25 ± 0.53	339.71 ± 5.04	337.38 ± 7.28	$H = 5.554$	$P = 0.062$
$CVV_{0-1\ mm}$	0.06 ± 0.01	0.06 ± 0.03	0.06 ± 0.02	$F = 0.007$	$P = 0.944$
$CVV_{0-3\ mm}$	0.68 ± 0.31	0.73 ± 0.36	0.71 ± 0.41	$F = 0.274$	$P = 0.823$
$CVV_{0-6\ mm}$	2.40 ± 0.98	2.51 ± 1.12	2.41 ± 1.29	$F = 0.202$	$P = 0.806$
$CVV_{0-9\ mm}$	4.83 ± 1.87	4.79 ± 2.05	4.49 ± 2.29	$F = 0.43$	$P = 0.548$
$CVV_{0-12\ mm}$	8.14 ± 2.78	7.48 ± 3.07	7.20 ± 3.63	$F = 1.177$	$P = 0.281$
$CVV_{0-15\ mm}$	11.83 ± 3.58	11.34 ± 3.50	10.04 ± 4.02	$F = 0.886$	$P = 0.509$
$CVV_{0-18\ mm}$	16.76 ± 4.77	15.66 ± 4.54	14.00 ± 5.39	$F = 0.948$	$P = 0.486$
$CVV_{0-21\ mm}$	21.94 ± 5.59	20.19 ± 5.65	18.31 ± 7.07	$F = 0.818$	$P = 0.557$
$CVI_{0-1\ mm}$	0.29 ± 0.01	0.27 ± 0.07	0.27 ± 0.07	$F = 0.202$	$P = 0.360$
$CVI_{0-3\ mm}$	0.29 ± 0.09	0.30 ± 0.09	0.30 ± 0.11	$F = 0.573$	$P = 0.586$
$CVI_{0-6\ mm}$	0.26 ± 0.07	0.28 ± 0.07	0.27 ± 0.08	$F = 1.788$	$P = 0.169$
$CVI_{0-9\ mm}$	0.24 ± 0.06	0.26 ± 0.07	0.24 ± 0.07	$F = 1.888$	$P = 0.099$
$CVI_{0-12\ mm}$	0.24 ± 0.05	0.26 ± 0.07	0.24 ± 0.07	$F = 1.321$	$P = 0.225$
$CVI_{0-15\ mm}$	0.33 ± 0.01	0.31 ± 0.04	0.28 ± 0.04	$F = 5.418$	$P = 0.013^{*}$
$CVI_{0-18\ mm}$	0.34 ± 0.01	0.32 ± 0.04	0.29 ± 0.04	$F = 5.039$	$P = 0.029$
$CVI_{0-21\ mm}$	0.35 ± 0.01	0.32 ± 0.04	0.30 ± 0.04	$F = 3.116$	$P = 0.081$
$CT_{0-1\ mm}$	313.50 ± 47.10	343.88 ± 107.40	343.39 ± 113.90	$F = 0.146$	$P = 0.946$
$CT_{0-3\ mm}$	337.29 ± 115.49	346.71 ± 95.98	340.32 ± 105.65	$F = 0.137$	$P = 0.601$
$CT_{0-6\ mm}$	323.24 ± 109.59	321.55 ± 88.36	317.67 ± 100.68	$F = 0.044$	$P = 0.926$
$CT_{0-9\ mm}$	301.11 ± 96.02	292.30 ± 78.47	289.26 ± 94.01	$H = 0.224$	$P = 0.894$
$CT_{0-12\ mm}$	288.42 ± 82.50	264.75 ± 67.27	273.89 ± 90.78	$H = 2.07$	$P = 0.355$
$CT_{0-15\ mm}$	249.70 ± 60.95	252.87 ± 66.72	242.57 ± 77.09	$F = 0.13$	$P = 0.846$
$CT_{0-18\ mm}$	240.28 ± 56.91	241.13 ± 59.13	230.67 ± 69.11	$F = 0.173$	$P = 0.853$
$CT_{0-21\ mm}$	231.07 ± 50.18	230.46 ± 52.72	220.02 ± 64.42	$F = 0.204$	$P = 0.805$

$^{*}P \leq 0.05$, $^{***}P \leq 0.001$.

$VD_{0-9\ mm}$: 0.124143). These results suggest that UWF PD remains a robust OCT parameter for effectively screening patients with DN from both T2DM and DR populations.

Subsequently, the UWF PD data underwent further processing using the 10-fold cross-validation method and random forest model to screen for DN within the T2DM and DR populations. The classification accuracy of each group in the 10-fold cross-validation method, along with the average classification accuracy of the random forest method, is presented in Table 6. The average classification accuracy of the random forest model for identifying patients with DN using PD was 85.8442% from the T2DM population and 82.5739% from the DR population.

Discussion

The complications of T2DM lead to a series of global health problems that persist over time. DR and DN are common microangiopathic complications in patients with long-term T2DM.[28] Microalbuminuria is an early marker of endothelial injury. Its presence significantly increases the risk of DR, indicating a shared pathophysiological mechanism[29] and a poten-

Table 5. Correlation Coefficients and Importance of Explanatory Variables by Random Forest Model for Screening DN Patients From the T2DM and DR Populations Using OCT Parameters

		T2DM Population		DR Population	
Serial Number	Explanatory Variable	*r* /*P* Value	Importance	*r* /*P* Value	Importance
1	$PD_{0–3\ mm}$	−0.481/0.000***	0.093891	−0.357/0.000***	0.075730
2	$PD_{0–6\ mm}$	−0.517/0.000***	0.086285	−0.384/0.000***	0.115155
3	$PD_{0–9\ mm}$	−0.507/0.000***	0.035642	−0.367/0.000***	0.079301
4	$PD_{0–12\ mm}$	−0.562/0.000***	0.251083	−0.397/0.000***	0.071463
5	$VD_{0–3\ mm}$	−0.415/0.000***	0.012599	−0.32/0.000***	0.000000
6	$VD_{0–6\ mm}$	−0.468/0.000***	0.081844	−0.361/0.000***	0.147807
7	$VD_{0–9\ mm}$	−0.441/0.000***	0.036460	−0.327/0.000***	0.124143
8	$VD_{0–12\ mm}$	−0.491/0.000***	0.089028	−0.360/0.000***	0.071463
9	$RT_{0–3\ mm}$	0.232/0.001***	0.012742	0.146/0.013*	0.012768
10	$RT_{0–6\ mm}$	0.395/0.000***	0.027245	0.273/0.000***	0.023990
11	$RT_{0–9\ mm}$	0.365/0.000***	0.058806	0.264/0.000***	0.000205
12	$RT_{0–12\ mm}$	0.301/0.000***	0.012904	0.226/0.000***	0.052941
13	$CP_{0–3\ mm}$	−0.280/0.000***	0.017138	−0.201/0.001***	0.000000
14	$CP_{0–6\ mm}$	−0.289/0.000***	0.004110	−0.208/0.000***	0.016227
15	$CP_{0–9\ mm}$	−0.223/0.001***	0.011474	−0.169/0.004**	0.013969
16	$CP_{0–12\ mm}$	−0.340/0.000***	0.021808	−0.233/0.000***	0.000047
17	$CVI_{0–3\ mm}$	−0.024/0.732	0.010929	−0.022/0.708	0.010172
18	$CVI_{0–6\ mm}$	−0.109/0.114	0.013494	−0.082/0.165	0.020079
19	$CVI_{0–9\ mm}$	−0.250/0.000	0.013467	−0.187/0.001	0.000512
20	$CVI_{0–12\ mm}$	−0.302/0.000***	0.069448	−0.207/0.000***	0.027629
21	$CVV_{0–3\ mm}$	0.064/0.354	0.000782	0.027/0.653	0.003248
22	$CVV_{0–6\ mm}$	0.011/0.873	0.031452	−0.007/0.905	0.002449
23	$CVV_{0–9\ mm}$	−0.046/0.501	0.026070	−0.041/0.488	0.003200
24	$CVV_{0–12\ mm}$	−0.105/0.126	0.004273	−0.075/0.203	0.000134
25	$CT_{0–3\ mm}$	0.078/0.256	0.005873	0.042/0.476	0.000000
26	$CT_{0–6\ mm}$	0.047/0.493	0.000475	0.026/0.664	0.000000
27	$CT_{0–9\ mm}$	0.011/0.879	0.000644	0.006/0.915	0.004981
28	$CT_{0–12\ mm}$	−0.018/0.796	0.001480	−0.011/0.847	0.003588

*$P \leq 0.05$, **$P \leq 0.01$, ***$P \leq 0.001$.

tial "common development path" between DR and DN.[30,31]

Due to challenges in accessing medical care and the uneven distribution of medical resources, telemedicine has gained unprecedented attention. Our team urgently needed to identify a simple and quick biomarker to screen for diabetic microvascular complications. The severity of DR correlates with the severity of DN, making it a potential marker for predicting the progression of chronic kidney disease. Many studies have evaluated the relationship between macular microvascular changes and the severity of DR in nephropathic patients using OCTA.[7,32–35] These studies also show that renal impairment, as a systemic risk factor, is associated with an enlarged FAZ area in diabetic patients.[7] As DN progresses, RVD gradually decreases[36] and the retinal microvasculature in both the superficial vascular plexus and deep vascular plexus becomes sparse.[37] Alé-Chilet et al.[38] reported that VD and FAZ areas can detect the degree of DN in patients with type 1 diabetes mellitus in a noninvasive and objective quantitative way. There is no potential advantage of PD in judging the type of DN.

In our research, compared with the control group, the average PD and VD of the DR without DN and DR with DN groups decreased significantly. Moreover, the decrease in PD and VD was significantly greater in the DR with DN group than in the DR without DN group. There was a correlation between UWF PD and DN diagnosis in both the T2DM and DR popula-

Table 6. Classification Accuracy of DN Patients From the T2DM and DR Populations Using Random Forest Method

Random Forest	T2DM Population, %	DR Population, %
Classification accuracy of 10-fold cross-validation	86.3636	82.7586
	86.3636	82.7586
	95.2381	82.7586
	90.4762	82.7586
	85.7143	82.7586
	85.7143	82.7586
	95.2381	82.7586
	80.9524	82.1429
	76.1905	82.1429
	76.1905	82.1429
Average classification accuracy of random forest	85.8442	82.5739

tions. This prompted us to consider whether UWF PD could be a reliable indicator for accurately screening DN. We used a deep learning method to analyze the UWF SS-OCT data, and the importance of explanatory variables by a random forest model between UWF PD and DN diagnosis from T2DM and DR populations was still high. The average classification accuracy of the random forest model for patients with DN screened out by PD was 85.8442% from the T2DM population and 82.5739% from the DR population. This suggests that UWF PD could be a quick and reliable biomarker for screening patients with DN from T2DM and DR populations using deep learning.

The diagnosis of DN typically depends on laboratory examination or renal biopsy, which is not optimal in terms of operational safety and cost-effectiveness. Patients with DR rarely realize the need for renal function examination.[39] Although FFA is the gold standard for detailed measurement of retinal microvasculature, this invasive procedure may increase the metabolic burden on patients with DN. With advancements in technology and multimodal imaging, OCTA achieves a higher blood vessel contrast than fundus photography and is not affected by dye leakage, which can obscure blood vessels in dye-based angiography.[21] Furthermore, UWF SS-OCTA offers a larger examination range and faster scanning speed,[40] allowing real-time and accurate assessment of peripheral retinal blood flow in DN patients. AI based on deep learning has garnered tremendous global interest recently.[41] By providing noninvasive, high-resolution, deep-resolution images of retinal and choroidal vessels, SS-OCTA significantly enhances our ability to use these images for disease screening and evaluating therapeutic efficacy and response.[21] Some scholars have used deep learning models to detect and predict the incidence of chronic kidney disease (CKD) from two-dimensional retinal fundus images.[42] Combining these superior biomarker detection capabilities with noninvasive procedures makes SS-OCTA, aided by deep learning, a promising screening technology for clinical practice.[21]

The BCVA (logMAR) of the DR without DN group and DR with DN group was significantly lower than that of the control group, with the reduction in the DR with DN group being greater. As T2DM progresses, retinal microvascular injury in DN patients worsens, leading to significant vision decline. In China, middle-aged and elderly patients often do not fully understand the complications of T2DM. It is important to note that vision decline can reflect DR progression in T2DM patients and warn of the possibility of DN, highlighting the need for disease awareness and screening.

Regarding choroidal indices, a meta-analysis by Kase et al.[43] indicated that monitoring choroidal vessels in diabetic eyes could help detect DR onset through longitudinal observation. However, there are still controversies about changes in CT and blood vessels in DR patients.[44,45] Studies have shown that CT is thinner and the choroidal vessel area is reduced in diabetic patients, while others have reported thicker CT and increased choroidal vessel area in DR patients.[46] One study found no difference in choroidal changes between the DR and control groups but did find differences between the DN and control groups.[47] The result was controversial. CVI and CVV are new quantitative parameters of choroidal vascular health.[48,49] Our research found that the CP ($CP_{0–3\ mm}$, $CP_{0–6\ mm}$, $CP_{0–9\ mm}$, $CP_{0–18\ mm}$) and CVI ($CVI_{0–15\ mm}$, $CVI_{0–18\ mm}$) decreased in patients from the DR without DN and DR with DN groups, but there was no significant difference in CT and CVV. We speculate that the decrease in CP may be related to the narrowing of choroidal arterioles, choriocapillaris atrophy, and capillary dropout. We aim to improve classification methods to explore the characteristics of choroidal microvasculature in DR and DN patients.

There are differing opinions on whether the duration of diabetes is a reliable predictor of DN.[50] Hung et al.[50] conducted a meta-analysis providing this view, while Sharma et al.[51] showed that diabetes duration was the strongest predictor of DN, with durations over 12 years being the best predictor. In our study, the duration of T2DM in the DR with DN group was 13.31 ± 6.4 years, compared to 9.53 ± 6.71 years in the DR without DN group. This supports the idea that when the duration of

T2DM exceeds 12 years, DN screening should be prioritized.

For ophthalmologists, early detection and diagnosis of DR and DN in T2DM patients should be emphasized. For patients with long duration of T2DM and DR, timely DN diagnosis is crucial to prevent DN progression, not just focusing on DR treatment. For endocrinologists, even without the guidance of ophthalmologists and nephrologists, UWF SS-OCTA provides a quick and reliable method to preliminarily assess DN in T2DM patients through AI. Monitoring UWF PD alleviates the pressure of uneven medical resource distribution and serves as a telemedicine-based screening scheme for T2DM complications.

There were some limitations to this study. First, the actual duration of T2DM may have been longer than recorded due to delayed diagnosis for various reasons. Despite our efforts to include DR at the same stage, strict differences between DR and DN existed according to different development stages. Additionally, we only included PD and VD for the deep vascular complex when collecting data. In the future, we will study the influence of PD on both the deep vascular complex and the superficial vascular complex in DN patients.

Conclusions

Our results suggest that when evaluating patients with DN in terms of retinal microvasculature, AI-guided UWF SS-OCTA detection of PD may serve as a rapid, reliable, and noninvasive early warning tool. Whether changes in choroidal microvasculature in patients with DR can be used as a predictive index remains to be verified. To positively impact the quality of life of T2DM patients, it is crucial to detect diabetic microvascular complications (DR and DN) as early as possible for implementing combined treatment strategies.

Acknowledgments

Supported by the Bethune Langmu Young Scholars Research Fund Project (BJ-LM2021007J) and New Ophthalmology Technology Incubation Fund Project.

The data sets used and/or analyzed during the current study are available from the corresponding author on reasonable request.

Disclosure: **X. Xie**, None; **W. Wang**, None; **H. Wang**, None; **Z. Zhang**, None; **X. Yuan**, None; **Y. Shi**, None; **Y. Liu**, None; **Q. Zhou**, None; **T. Liu**, None

[*] XX and WW contributed equally to this work and share first authorship.

References

1. Cho NH, Shaw JE, Karuranga S, et al. IDF Diabetes Atlas: global estimates of diabetes prevalence for 2017 and projections for 2045. *Diabetes Res Clin Pract*. 2018;138:271–281.
2. Faselis C, Katsimardou A, Imprialos K, Deligkaris P, Kallistratos M, Dimitriadis K. Microvascular complications of type 2 diabetes mellitus. *Curr Vasc Pharmacol*. 2020;18(2):117–124.
3. Qi C, Mao X, Zhang Z, Wu H. Classification and differential diagnosis of diabetic nephropathy. *J Diabetes Res*. 2017;2017:8637138.
4. Nusinovici S, Sabanayagam C, Lee KE, et al. Retinal microvascular signs and risk of diabetic kidney disease in Asian and white populations. *Sci Rep*. 2021;11(1):4898.
5. Cho A, Park HC, Lee YK, Shin YJ, Bae SH, Kim H. Progression of diabetic retinopathy and declining renal function in patients with type 2 diabetes. *J Diabetes Res*. 2020;2020:8784139.
6. Hung CC, Lin HY, Hwang DY, et al. Diabetic retinopathy and clinical parameters favoring the presence of diabetic nephropathy could predict renal outcome in patients with diabetic kidney disease. *Sci Rep*. 2017;7(1):1236.
7. Ahmadzadeh Amiri A, Sheikh Rezaee MR, Ahmadzadeh Amiri A, Soleymanian T, Jafari R, Ahmadzadeh Amiri A. Macular optical coherence tomography angiography in nephropathic patients with diabetic retinopathy in Iran: a prospective case-control study. *Ophthalmol Ther*. 2020;9(1):139–148.
8. Zhang J, Wang Y, Li L, et al. Diabetic retinopathy may predict the renal outcomes of patients with diabetic nephropathy. *Ren Fail*. 2018;40(1):243–251.
9. Laíns I, Wang JC, Cui Y, et al. Retinal applications of swept source optical coherence tomography (OCT) and optical coherence tomography angiography (OCTA). *Prog Retin Eye Res*. 2021;84:100951.
10. Liu T, Lin W, Shi G, et al. Retinal and choroidal vascular perfusion and thickness measurement in diabetic retinopathy patients by the swept-source

optical coherence tomography angiography. *Front Med (Lausanne)*. 2022;9:786708.
11. Bermejo S, Pascual J, Soler MJ. The current role of renal biopsy in diabetic patients. *Minerva Med*. 2018;109(2):116–125.
12. Chatterjee S, Khunti K, Davies MJ. Type 2 diabetes. *Lancet*. 2017;389(10085):2239–2251.
13. Yang Z, Tan TE, Shao Y, Wong TY, Li X. Classification of diabetic retinopathy: past, present and future. *Front Endocrinol (Lausanne)*. 2022;13:1079217.
14. Haneda M, Utsunomiya K, Koya D, et al. A new classification of diabetic nephropathy 2014: a report from Joint Committee on Diabetic Nephropathy. *Clin Exp Nephrol*. 2015;19(1):1–5.
15. Ha M, Choi SY, Kim M, Na JK, Park YH. Diabetic nephropathy in type 2 diabetic retinopathy requiring panretinal photocoagulation. *Korean J Ophthalmol*. 2019;33(1):46–53.
16. Yang J, Wang E, Yuan M, Chen Y. Three-dimensional choroidal vascularity index in acute central serous chorioretinopathy using swept-source optical coherence tomography. *Graefes Arch Clin Exp Ophthalmol*. 2020;258(2):241–247.
17. Cao Y, Zhang Y, Gu X, Zhu D, Yang L. Choroid vascular changes in hyperopic anisometropia amblyopia using SS-OCTA. *BMC Ophthalmol*. 2023;23(1):379.
18. Kostic M, Bates NM, Milosevic NT, et al. Investigating the fractal dimension of the foveal microvasculature in relation to the morphology of the foveal avascular zone and to the macular circulation in patients with type 2 diabetes mellitus. *Front Physiol*. 2018;9:1233.
19. Mititelu M, Uschner D, Doherty L, et al. Retinal thickness and morphology changes on OCT in youth with type 2 diabetes: findings from the TODAY study. *Ophthalmol Sci*. 2022;2(4):100191.
20. Hormel TT, Hwang TS, Bailey ST, Wilson DJ, Huang D, Jia Y. Artificial intelligence in OCT angiography. *Prog Retin Eye Res*. 2021;85:100965.
21. Hormel TT, Jia Y. OCT angiography and its retinal biomarkers [Invited]. *Biomed Opt Express*. 2023;14(9):4542–4566.
22. Abadia B, Suñen I, Calvo P, Bartol F, Verdes G, Ferreras A. Choroidal thickness measured using swept-source optical coherence tomography is reduced in patients with type 2 diabetes. *PLoS One*. 2018;13(2):e0191977.
23. Hormel TT, Huang D, Jia Y. Artifacts and artifact removal in optical coherence tomographic angiography. *Quant Imaging Med Surg*. 2021;11(3):1120–1133.
24. Li C, Yuan Y, Kong X, et al. Segmentation errors and off-center artifacts in SS-OCT: insight from a population-based imaging study. *Curr Eye Res*. 2023;48(10):949–955.
25. Park S, Hong M, Lee H, et al. New model for predicting the presence of coronary artery calcification. *J Clin Med*. 2021;10(3):457.
26. Mantero A, Ishwaran H. Unsupervised random forests. *Stat Anal Data Min*. 2021;14(2):144–167.
27. Schmidt LJ, Rieger O, Neznansky M, et al. A machine-learning-based algorithm improves prediction of preeclampsia-associated adverse outcomes. *Am J Obstet Gynecol*. 2022;227(1):77.e1–77.e30.
28. Li Y, Su X, Ye Q, et al. The predictive value of diabetic retinopathy on subsequent diabetic nephropathy in patients with type 2 diabetes: a systematic review and meta-analysis of prospective studies. *Ren Fail*. 2021;43(1):231–240.
29. Chen Y, Qi Z, Hou X, Chen L. Optical coherence tomography angiography for assessment of changes of the retina and choroid in different stages of diabetic retinopathy and their relationship with diabetic nephropathy. *Endokrynol Pol*. 2023;74(2):135–139.
30. He F, Xia X, Wu XF, Yu XQ, Huang FX. Diabetic retinopathy in predicting diabetic nephropathy in patients with type 2 diabetes and renal disease: a meta-analysis. *Diabetologia*. 2013;56(3):457–66.
31. Zhao X, Liu Y, Zhang W, et al. Relationships between retinal vascular characteristics and renal function in patients with type 2 diabetes mellitus. *Transl Vis Sci Technol*. 2021;10(2):20.
32. Ahmed MH, Elwali ES, Awadalla H, Almobarak AO. The relationship between diabetic retinopathy and nephropathy in Sudanese adult with diabetes: population based study. *Diabetes Metab Syndr*. 2017;11(suppl 1):S333–S336.
33. Cao X, Gong X, Ma X. Diabetic nephropathy versus diabetic retinopathy in a chinese population: a retrospective study. *Med Sci Monit*. 2019;25:6446–6453.
34. Jawa A, Kcomt J, Fonseca VA. Diabetic nephropathy and retinopathy. *Med Clin North Am*. 2004;88(4):1001–1036, xi.
35. Edwards MS, Wilson DB, Craven TE, et al. Associations between retinal microvascular abnormalities and declining renal function in the elderly population: the Cardiovascular Health Study. *Am J Kidney Dis*. 2005;46(2):214–224.
36. Cankurtaran V, Inanc M, Tekin K, Turgut F. Retinal microcirculation in predicting diabetic nephropathy in type 2 diabetic patients without

retinopathy. *Ophthalmologica*. 2020;243(4):271–279.

37. Yeung L, Wu IW, Sun CC, et al. Early retinal microvascular abnormalities in patients with chronic kidney disease. *Microcirculation*. 2019;26(7):e12555.
38. Alé-Chilet A, Bernal-Morales C, Barraso M, et al. Optical coherence tomography angiography in type 1 diabetes mellitus-report 2: diabetic kidney disease. *J Clin Med*. 2021;11(1):197.
39. Samsu N. Diabetic nephropathy: challenges in pathogenesis, diagnosis, and treatment. *Biomed Res Int*. 2021;2021:1497449.
40. Kim K, You JI, Park JR, Kim ES, Oh WY, Yu SY. Quantification of retinal microvascular parameters by severity of diabetic retinopathy using wide-field swept-source optical coherence tomography angiography. *Graefes Arch Clin Exp Ophthalmol*. 2021;259(8):2103–2111.
41. Ting DSW, Pasquale LR, Peng L, et al. Artificial intelligence and deep learning in ophthalmology. *Br J Ophthalmol*. 2019;103(2):167–175.
42. Zhang K, Liu X, Xu J, et al. Deep-learning models for the detection and incidence prediction of chronic kidney disease and type 2 diabetes from retinal fundus images. *Nat Biomed Eng*. 2021;5(6):533–545.
43. Kase S, Endo H, Takahashi M, et al. Choroidal vascular structures in diabetic patients: a meta-analysis. *Graefes Arch Clin Exp Ophthalmol*. 2021;259(12):3537–3548.
44. Kase S, Endo H, Takahashi M, et al. Alteration of choroidal vascular structure in diabetic retinopathy. *Br J Ophthalmol*. 2020;104(3):417–421.
45. Adhi M, Brewer E, Waheed NK, Duker JS. Analysis of morphological features and vascular layers of choroid in diabetic retinopathy using spectral-domain optical coherence tomography. *JAMA Ophthalmol*. 2013;131(10):1267–1274.
46. Gupta P, Thakku SG, Sabanayagam C, et al. Characterisation of choroidal morphological and vascular features in diabetes and diabetic retinopathy. *Br J Ophthalmol*. 2017;101(8):1038–1044.
47. Kocasarac C, Yigit Y, Sengul E, Sakalar YB. Choroidal thickness alterations in diabetic nephropathy patients with early or no diabetic retinopathy. *Int Ophthalmol*. 2018;38(2):721–726.
48. Foo VHX, Gupta P, Nguyen QD, et al. Decrease in choroidal vascularity index of Haller's layer in diabetic eyes precedes retinopathy. *BMJ Open Diabetes Res Care*. 2020;8(1):e001295.
49. Han X, Du NN, Li S, Diao ZL, Fu L, Liu WH. Choroidal vascularity index assessment: a potential non-invasive technique for diagnosing diabetic nephropathy. *J Ophthalmol*. 2022;2022:3124746.
50. Hung CC, Lin HY, Hwang DY, et al. Diabetic retinopathy and clinical parameters favoring the presence of diabetic nephropathy could predict renal outcome in patients with diabetic kidney disease. *Sci Rep*. 2017;7(1):1236.
51. Sharma SG, Bomback AS, Radhakrishnan J, et al. The modern spectrum of renal biopsy findings in patients with diabetes. *Clin J Am Soc Nephrol*. 2013;8(10):1718–1724.